This research was conducted at the University of Lille in collaboration with several French institutions (CNRS, INSERM, INRAE) and international partners (Tokyo University of Science and Doshisha University, Japan).

The effect of humidity, temperature, and drying duration on microparticle detachment force: insights into capillary-induced deformation at the particle–substrate interface

In this study, we reveal how drying conditions of an evaporating capillary bridge between a 2-μm microparticle and a substrate can squeeze the particle against the surface, enlarging the contact zone and strengthening adhesion.

Image reproduced by permission of Farzam Zoueshtiagh from *Soft Matter*, 2026, **22**, 2249.

ROYAL SOCIETY OF CHEMISTRY

rsc.li/soft-matter-journal

The effect of humidity, temperature, and drying duration on microparticle detachment force: insights into capillary-induced deformation at the particle–substrate interface

Javad Sherafatpour, [ID] [ag] Anna Ipatova, [ID] [a] Alexis Duchesne, [ID] [a]
H. N. Yoshikawa, [ID] [bh] Pascal Mariot, [ID] [c] Christine Faille, [ID] [d] Ichiro Ueno, [ID] [e]
Georg F. Dietze [ID] [f] and Farzam Zoueshtiagh [ID] *[a]

We experimentally investigate how drying history influences microparticle–substrate adhesion in hydrophilic systems. By systematically varying air temperature, relative humidity, and drying duration under controlled conditions, we quantify the detachment force of individual microparticles. Air temperature emerges as the dominant factor: higher temperatures and lower humidity enhance adhesion, while prolonged drying generally reduces it, except under combined high-temperature and low-humidity conditions, where strong adhesion persists. Complementary scanning electron microscopy (SEM) results reveal drying-time-dependent changes in the particle–substrate contact size, consistent with capillary-induced compression of the contact zone followed by partial relaxation. These findings indicate that transient capillary stresses during evaporation deform the particle–substrate interface and leave a lasting imprint on adhesion strength. Overall, the study shows how capillarity, drying dynamics, and contact mechanics couple to regulate adhesion in colloidal systems, offering new insights into particle–substrate interactions in soft matter contexts.

1 Introduction

Microscopic particles or dirt, although invisible to the naked eye, can have a notable impact on our daily lives. Their presence is a common concern in different sectors, like the food industry where they act as contaminants, or in microelectronics where they may pose a risk of flawed microfabrication. Their removal is, therefore, crucial in application domains ranging from microtechnology,[1–4] automotive[5,6] to food[7–10] industries. Yet cleaning technologies must be improved to reduce energy consumption as well as the use of water and detergents.[11] Achieving efficient cleaning with minimal energy input is closely linked to understanding and controlling the adhesion of dirt to the substrate.

The relevance of adhesion mechanisms extends well beyond dirt removal. Similar physical processes also govern particle–particle and particle–substrate interactions in drying systems, where adhesion plays a central role in phenomena such as cracking, delamination, and peeling of drying deposits. In particular, the adhesion of colloidal particles to a solid substrate during droplet evaporation has been shown to strongly influence crack morphology and delamination pathways.[12,13] These effects are of fundamental importance in coating technologies, where controlling adhesion during drying is essential for ensuring mechanical integrity and performance.

Adhesion arises from a complex interplay of van der Waals forces, capillary bridges, electrostatic interactions, and mechanical interlocking. Theoretical descriptions have long relied on contact mechanics models, most notably the Johnson–Kendall–Roberts (JKR)[14] and Derjaguin–Muller–Toporov (DMT)[15] theories, which describe adhesive contact between elastic bodies. The JKR model applies to soft, highly adhesive materials, whereas the DMT model is better suited to stiff, weakly adhesive ones. Maugis[16] bridged these regimes with the Dugdale cohesive zone model, and later refinements[17,18] incorporated roughness and viscoelasticity. Despite these advances, such

[a] *Univ. Lille, CNRS, ECLille, ISEN, Univ. Valenciennes, UMR 8520 – IEMN, F-59000 Lille, France. E-mail: farzam.zoueshtiagh@univ-lille.fr*

[b] *Université Côte d'Azur, CNRS, Institut de Physique de Nice, 06100 Nice, France*

[c] *Univ. Lille, INSERM U1003, Bâtiment SN3, F-59655 Villeneuve d'Ascq, France*

[d] *Univ. Lille, CNRS, INRAE, ENSCL, UMET, F-59650 Villeneuve d'Ascq, France*

[e] *Department of Mechanical and Aerospace Engineering, Faculty of Science and Technology, Tokyo University of Science, Chiba 278-8510, Japan*

[f] *Université Paris-Saclay, CNRS, FAST, 91405 Orsay, France*

[g] *Institut de Mécanique des Fluides de Toulouse, Université de Toulouse, UMR 5502, CNRS-INPT-UPS, 31400 Toulouse, France*

[h] *Faculty of Science and Engineering, Doshisha University, 1-3 Tatara Miyakodani, Kyotanabe-shi, Kyoto 610-0321, Japan*

models remain essentially static and are unable to capture the dynamic, history-dependent nature of adhesion. A typical situation in real systems occurs when a dirt particle, initially suspended in a liquid, becomes deposited on a surface following evaporation of the surrounding fluid. During drying, the contact area evolves and a liquid bridge forms between the particle and the substrate before eventually collapsing. As a result, the adhesion force between a particle and a substrate can be strongly influenced by the environmental conditions prevailing during particle deposition and drying. Yet, despite its relevance, the influence of drying history on subsequent adhesion has been only scarcely investigated, aside from a few notable studies.

Several studies have examined the environmental conditions during the evaporative phase on the adhesion.[19–22] Faille et al.[19] demonstrated that temperature and the duration of particle residence on a surface significantly affect the detachment force. Shiri et al.[20] reported that temperature and humidity modulate adhesion in pressure-sensitive adhesive films by altering the evaporation rate, surface roughness, and internal cohesion. Thill and Spalla,[21] as well as Endo et al.,[22] highlighted the critical role of capillary bridges in determining both deposition morphology and adhesion strength. However, these studies primarily focused on isolated parameters and did not provide a comprehensive understanding of how drying-induced adhesion evolves dynamically under coupled environmental effects.

To address this gap, the present study investigates how evaporation—and the associated formation of liquid bridges—affects the adhesion of a microparticle at its contact zone with a substrate. To this end, samples of particle suspensions are dried under controlled environmental conditions before being immersed for detachment force measurements using a custom-built setup. This configuration mimics practical cleaning processes, in which dirt particles typically undergo an immersion phase following a prior drying step.

Once immersed, we experimentally measure the detachment force of individual microparticles and demonstrate that adhesion depends strongly on the environmental history preceding detachment. Complementary SEM observations further reveal variations in contact geometry that reflect the influence of the drying process.

To isolate the specific role of drying, we focus exclusively on hydrophilic particles and hydrophilic substrates. This choice is motivated by our recent findings showing that the wetting properties of the interacting surfaces strongly influence adhesion forces during detachment.[11,23] In particular, we previously demonstrated that the presence of a trapped bubble at the particle–substrate interface can introduce additional capillary forces, but that such entrapment is not expected to be prevalent when both surfaces are hydrophilic. While surface roughness may modify the apparent wettability through contact-line pinning and could, in some cases, promote bubble trapping, the particle–substrate combinations investigated here were selected to minimize this effect. Under these conditions, bubble entrapment is therefore considered unlikely, allowing us to focus on how environmental drying parameters—namely relative humidity, air temperature, and drying duration—govern the detachment force measured after drying.

2 Experimental

We first present the methodology used to carry out the drying stage of microparticles initially dispersed in a water droplet. The method details the steps taken while maintaining precise control over both temperature and relative air humidity. We next provide details on the protocol to carry out the experiments that permitted us to estimate the force required to detach a particle from a surface.

2.1 Methods and materials

To investigate the effect of drying conditions on microparticle detachment from the substrate, we employed a climate chamber (Memmert HPC50), which allows for controlled regulation of temperature (from 35 to 90 °C) and relative humidity (from 20 to 90%). Preliminary tests were conducted to verify the chamber's ability to accurately maintain the prescribed temperature and humidity levels, as well as to determine the stabilization time required to reach the setpoints. This stabilization period ranged from approximately 10 min under the most favorable conditions (low humidity combined with high temperature) to about 30 min under the least favorable conditions (high humidity combined with low temperature). Based on these assessments, the experimental range was set to temperatures between 35 °C and 80 °C as well as relative humidity between 20% and 80%.

We used hydrophilic silver coated silica microspheres (SiO2MS-AG-4.1, Cospheric) having a diameter of 2 μm (coefficient of variation = 3.3%) with a density of 4.1 g cm^{-3}. The particle contact angle was measured using the method of placing a droplet on a lawn of particles.[24] Briefly, we passed 1.5 mL of particle suspension through a filter (cellulose esters 0.025 μm) to form a dense lawn of particles. Then, a water droplet was placed on this lawn and the contact angle measured using an optical tensiometer (Biolin Theta Lite) in "sessile drop" mode to measure static contact angle. The same optical tensiometer was used to measure the substrate contact angle. The static contact angle, measured for silver-coated silica microspheres and the glass substrate (coverslip) that was previously cleaned with isopropanol, was determined to be 10° ± 4° and 39° ± 1°, respectively. The coverslips were cleaned by sequential rinsing with isopropanol and deionized water, followed by drying in an oven at 40 °C for 10 minutes. After cooling to room temperature, droplets containing microparticles were deposited onto the cleaned coverslips, which were then placed in the climate chamber.

16.2 mg of particles were dispersed in 5 ml of de-ionized water, resulting in a concentration of approximately 1.9×10^8 particles per milliliter. While the concentration was not a critical factor in the experiments, it was selected to avoid situations with densely packed particles on the substrate or very few particles for measuring the detachment force. A drop

of this suspension was placed on the coverslip which was thereafter placed into the chamber for controlled drying. To maintain consistent droplet sizes throughout all experiments conducted across various temperature and humidity ranges, we standardized the droplet size containing the microparticles to 4 μL. This volume guaranteed a swift and complete evaporation of the droplet within a few minutes, even under the least favorable conditions of high humidity and low temperatures. This complete evaporation time was at least one order of magnitude smaller than the shortest investigated duration, *viz.* 24 h, after which the test cell was removed from the chamber to measure the detachment force. It should be emphasized that the term that will be used throughout the manuscript "drying duration" will refer to the total environmental exposure time during which the droplet dries and the particle–substrate contact evolves. As will be seen, the measured detachment forces do not necessarily correspond to an equilibrium state, even at the longest exposure times investigated.

After removing the coverslip from the chamber and allowing it to cool to room temperature, we carefully poured 4 mL of Hanks' balanced salt solution (HBSS†)[25] to fully immerse the particles. To prevent loosely adhered particles from floating, this immersion step was performed twice: after the initial addition of HBSS, we gently removed the solution, thereby discarding any non-adherent particles and then replenished the sample with a fresh 4 mL of HBSS before proceeding with detachment force measurements.

Afterwards, the coverslip is positioned within a vacuum chamber (Nalgene, volume 4.7 L; vacuum pump Laboport N 86 KN.18) for a duration of 60 minutes. Although the manufacturer's specifications indicated that the pump achieves a maximum vacuum level of approximately 100 mbar after around 10 minutes for our 4.7 L vacuum chamber, our pressure measurements revealed that it took approximately 15 minutes to reach the targeted vacuum level of 100 mbar. The prolonged degassing time integrated into our experiments aimed to eliminate any excess gas within the HBSS solution. This meticulous degassing procedure was specifically devised to prevent any potential entrapment of bubbles beneath a particle, which could interfere with the measurement of detachment force.[23]

2.2 Detachment force measurement

The detachment force measurement procedure draws inspiration from the patch-clamp technique,[26] albeit with modifications. Rather than using a voltage difference for clamping, we employ flow depression. Traditionally, the patch-clamp technique involves a pipette filled with an electrolyte solution and an electrode, interacting with a cell submerged in a bath containing a ground electrode. Voltage is applied to clamp the cell, and researchers monitor ionic currents using connected electrodes and an amplifier. In our adaptation, we exclusively utilize
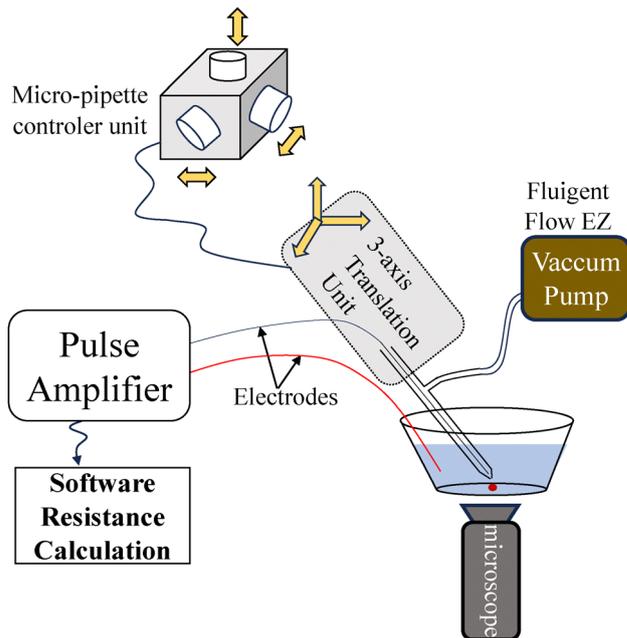

Fig. 1 Schematic of the patch-clamp setup used in this work. In a traditional patch-clamp setup the vacuum pump is not present.

electrodes to assess the electrical resistance of the pipette, aiming to determine its tip size[11,23] (for detailed information on the calibration process correlating the tip size with the resistance, refer to S1).

A schematic illustration of the setup is shown in Fig. 1. A controlled flow depression (Fluigent LineUp Flow EZ) is directed through the pipette when its tip closely approaches the microbead's surface. Subsequently, the pipette is vertically moved away from the particle at a specified speed (3 μm s^{-1}). The inverted microscope monitors from beneath the particle's response in real-time. If the particle remains affixed to the substrate without detachment, signifying non-detachment, we re-approach the micropipette and apply increased aspiration pressure. This iterative process continues until the particle detaches (Fig. 2). The minimum pressure required for detachment, considering the surface area of the pipette's tip, yields the corresponding force needed to dislodge the particle from the substrate (refer to S2 for details). The difference between the detachment pressure and the last pressure at which the detachment process failed is regarded as the uncertainty zone. An illustrative video of the particle detachment process is included as Video S3. It is important to note that, after the drying step in the climate chamber, particles formed a ring-shaped deposit characteristic of the coffee-ring effect.[27] Detachment force measurements were carried out solely on well-isolated particles (as shown in Fig. 2), typically located away from the dense peripheral region of the deposit. This approach was adopted to prevent interactions with neighboring particles and avoid collective effects.

We employed a 3-inch length, 1.5 mm diameter single capillary with a filament sourced from "World Precision Instruments". This capillary was drawn using the P-97 Flaming/Brown Micropipette Puller from "Sutter Instruments". With the ability to
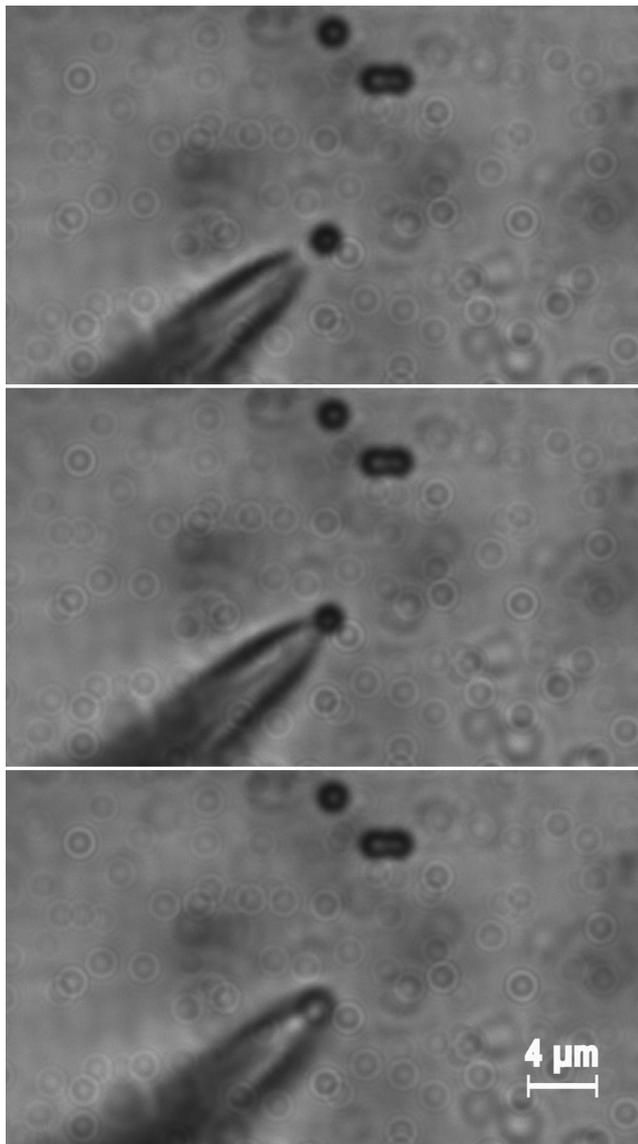
---

† HBSS is commonly used as a buffer in cell culture media to maintain osmotic pressure and physiological pH. Its composition (in mmol) is: 142 NaCl, 5.6 KCl, 1 CaCl$_2$, 1 MgCl$_2$, 10 HEPES, 2 NaHCO$_3$, 0.44 KH$_2$PO$_4$, and 0.34 Na$_2$HPO$_4$, with an osmolarity of 300 mOsm L^{-1} and pH 7.4.

Fig. 2 Micro-pipette approaching an individual microparticle (top). Suction is applied *via* controlled under pressure within the pipette channel (middle). The particle is subsequently detached and lifted by the pipette (bottom).

modify the micro-pipette's tip, we developed five distinct programs to pull the capillary tube at varying velocities and temperatures, facilitating the creation of diverse micro-pipette tips. In contrast to prior studies where the micro-pipette surface remained fixed for specific particle sizes,[11] our approach involved modifying the micro-pipette tip size to regulate the force applied to the particle. This adjustment allowed us to enhance precision by reducing the uncertainty zones, especially in situations where particle detachment occurred under low pressure.

For each detachment curve, at least 22 individual particles were dislodged from the same substrate. Particular care was taken to select well-isolated particles to avoid any collective or neighboring effects that could bias the measurements. Additionally, to prevent re-capturing an already detached particle,

the pipette was fully withdrawn from the sample after each detachment while maintaining the same aspiration pressure used during the removal. A new pipette was then installed in the system before proceeding with the next measurement.

3 Results

As previously mentioned, our focus in this study revolves around analyzing the impact of temperature, humidity and drying duration on detachment force. Each experiment was conducted under constant conditions, with only one parameter altered at a time. This approach enables us to delineate and comprehend the individual effects of each parameter.

Prior to presenting the main results, it is essential to emphasize that the repeatability of our measurements was carefully verified. To this end, tests were conducted on distinct samples, each subjected to identical drying conditions. Fig. 3 presents the comparison: experimental data points are shown as symbols, while solid lines represent a nonlinear least squares fit to the data using the logistic function:

$$P(x) = \frac{100 \cdot \left(e^{bx} - 1\right)}{e^{bx} - c}, \qquad (1)$$

where $b > 0$ and $c < 0$ are fitting parameters, x denotes the applied force (in nN), and $P(x)$ corresponds to the percentage of particles removed at that force. As illustrated in Fig. 3, only minor variations were observed across the samples, confirming the robustness and reproducibility of the experimental procedure.

Fig. 4–7 shows the effect of various drying conditions. Each figure comprises a primary large plot displaying experimental data points as well as the fitted logistic function as the solid lines, complemented by a smaller subplot below. The subplots are the derivatives of the determined fitting function $P(x)$ whose fitting coefficients, b and c are given in S4. They illustrate the dispersion and range of measured forces under a specific experimental condition.
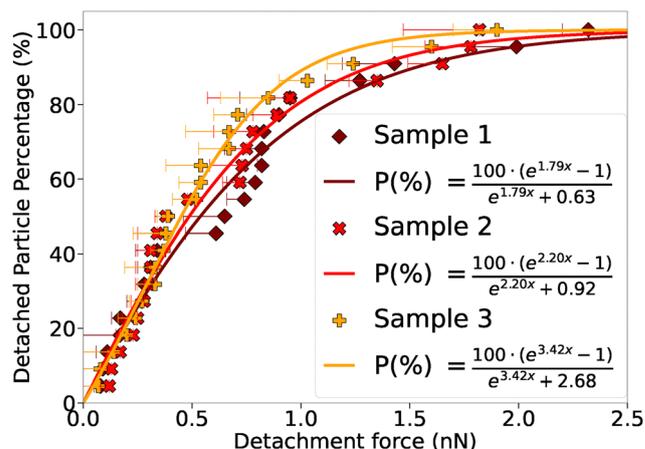

Fig. 3 Verification of measurement repeatability: detachment force measured for three different samples dried under identical conditions ($\Delta t = 24$ h, $T = 35\ ^{\circ}$C, $H = 80$%).
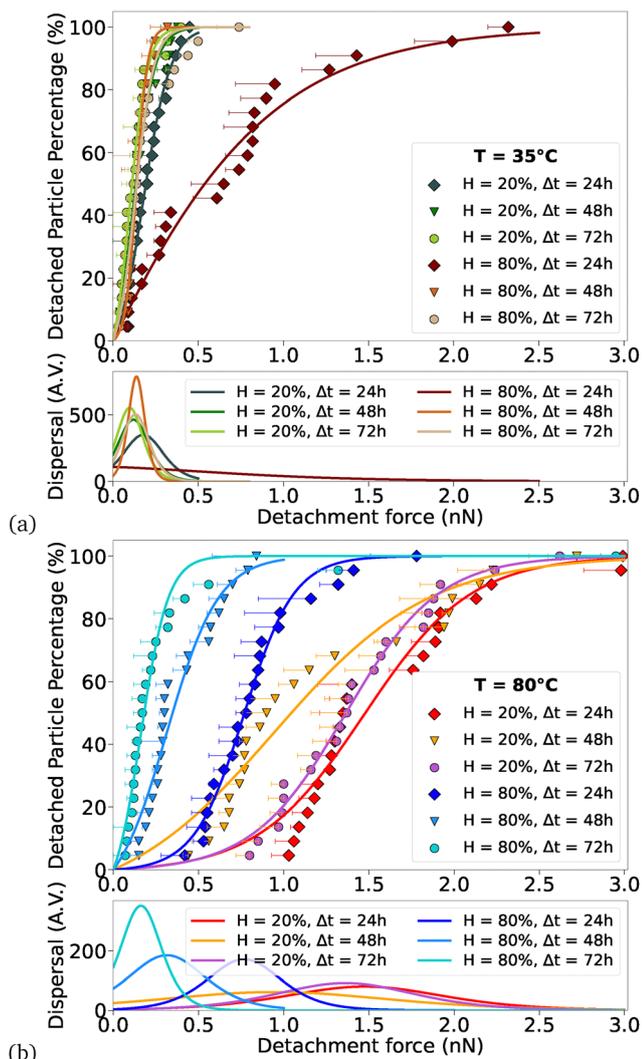
Fig. 4 Effect of humidity and drying time variation (Δt) on detachment force under constant temperatures of (a) 35 °C and (b) 80 °C. Solid lines in the main plot represent fitted logistic functions.
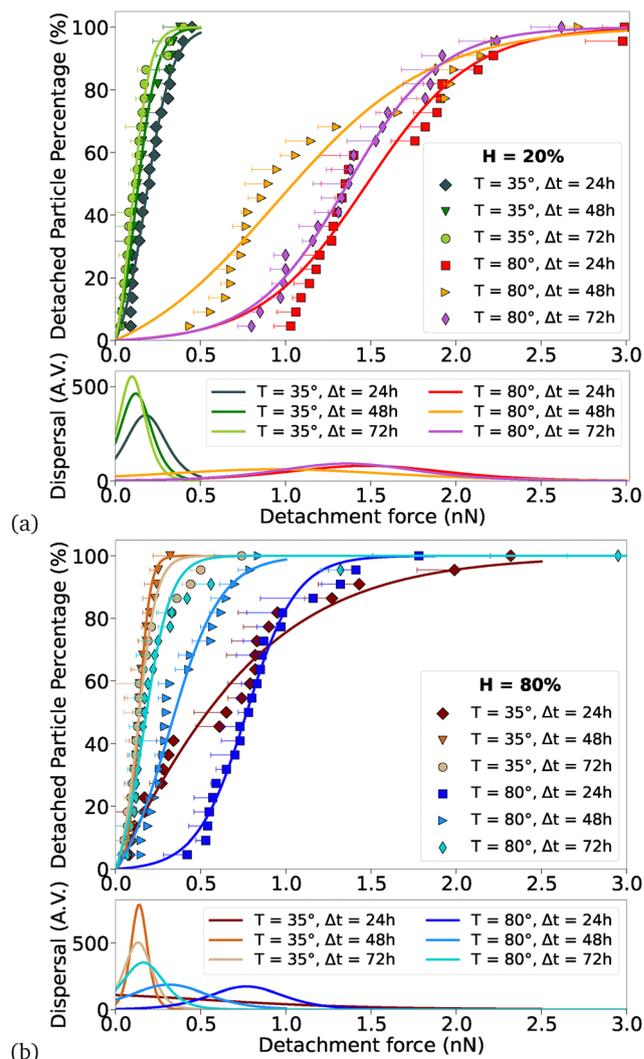

Fig. 5 Effect of temperature and drying time variation (Δt) on the detachment force under constant relative humidity of (a) H = 20% and (b) H = 80%. Solid lines in the main plot represent fitted logistic functions.

Fig. 4 and 5 examine the influence of drying conditions on particle detachment. Specifically, we investigate the effect of humidity levels (H = 20% and H = 80%) in Fig. 4, and the effect of temperatures (T = 35 °C and T = 80 °C) in Fig. 5, each across three drying durations (Δt = 24 h, 48 h, and 72 h). In each case, one parameter, either temperature or humidity, is held constant to isolate the impact of the other. A consistent color-coded scheme is used to distinguish between the datasets, which appear in both figures for ease of comparison under varying conditions.

3.1 Effect of humidity and drying time Δt

Fig. 4(a) and (b) depict the impact of humidity and drying time variation (Δt) on detachment force at temperatures of 35 °C and 80 °C, respectively.

In Fig. 4(a), the data at H = 20% (depicted in green tones) demonstrate a slight decrease with increasing Δt. This decline is more noticeable when observing the data dispersion on the

smaller plot, where the peak of Gaussian distributions shifts toward smaller detachment forces as Δt increases. The scenario for H = 80% (in brown hues) is more intricate, showcasing substantial variations in detachment force when measured at 24 h compared to 48 or 72 h. Notably, the values of the detachment force, F_{d}, at Δt = 24 h extend up to approximately 2.5 nN, while they remain below 0.5 nN for Δt = 48 h and Δt = 72 h. Moreover, the data from Δt = 48 h and Δt = 72 h exhibit close proximity, appearing almost indistinguishable—a similarity supported by the shape and position of their corresponding Gaussian functions in the smaller plot. Finally, the Gaussian spread of the data at Δt = 24 h seems notably wide, while the other datasets exhibit relatively smaller standard deviations.

In Fig. 4(b), where the temperature remains constant at 80 °C, the influence of drying time is evident for both tested relative humidity levels of H = 20% (depicted in red tones) and H = 80% (in blue hues). A consistent decline is observed from Δt = 24 h to Δt = 72 h for H = 80%, showcasing a Gaussian
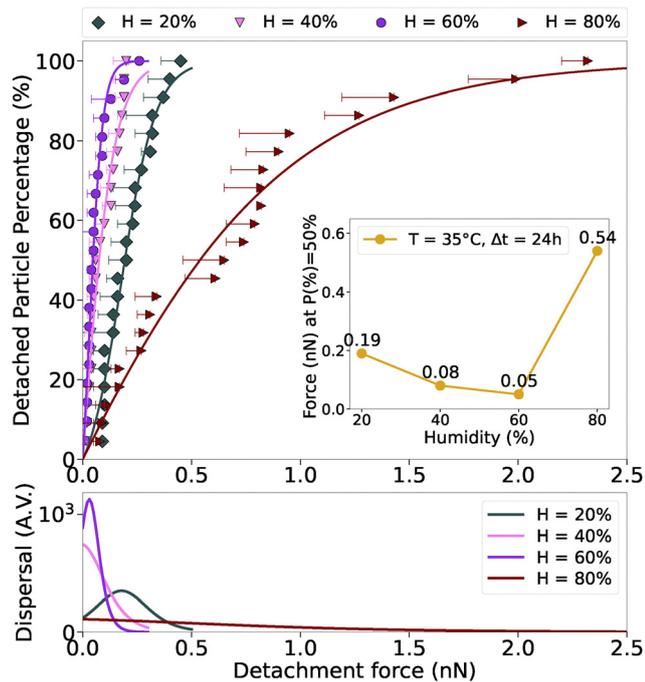
Fig. 6 Effect of humidity under constant drying time (Δt = 24 h) and temperature (T = 35 °C). Solid lines in the main plot represent fitted logistic functions.
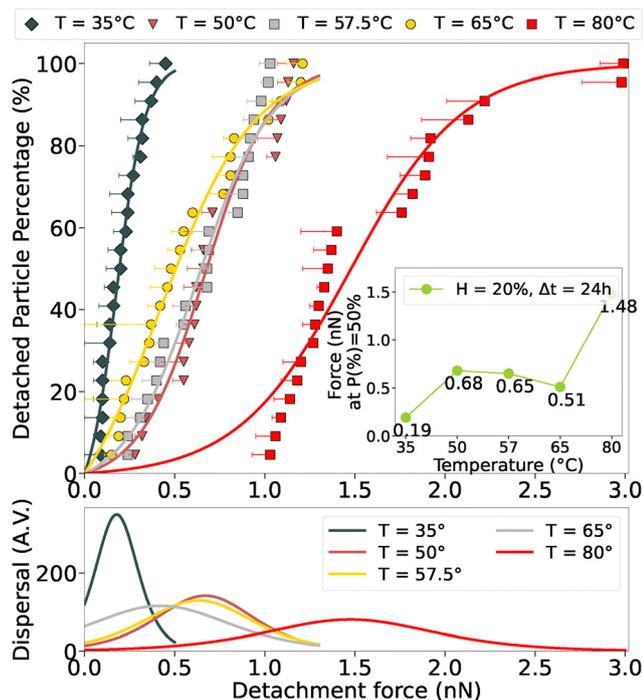

Fig. 7 Effect of temperature under constant drying time (Δt = 24 h) and relative humidity (H = 20%). Solid lines in the main plot represent fitted logistic functions.

function with the smallest standard deviation at Δt = 72 h. Conversely, at the lower relative humidity of H = 20%, not only are the data values generally larger than those of H = 80%, but

they also display more spread and exhibit 'flattened' Gaussian distributions. Additionally, the measured F_d data initially show a decline when Δt changes from 24 h to 72 h, but surprisingly, they rebound to values nearly matching those at 24 h.

3.2 Effect of temperature and drying time Δt

Fig. 5(a) and (b) illustrate the influence of temperature and drying duration (Δt) on the detachment force at constant humidity levels of H = 20% and H = 80%, respectively. In Fig. 5(a), the data corresponding to T = 35 °C (shown in green tones) replicate those in Fig. 4(a), enabling direct comparison with the results obtained at T = 80 °C. A slight and consistent decrease in detachment force with increasing Δt is observed for both temperatures. However, a striking difference emerges: higher drying temperatures lead to substantially larger detachment forces (up to an order of magnitude greater) compared to the lower temperature condition. Fig. 5(b) presents the same comparison at H = 80%. Here, the detachment force F_d is higher at shorter drying durations. At T = 80 °C, F_d consistently exceeds the corresponding values measured at T = 35 °C for each drying duration Δt. This highlights the strong influence of temperature on particle adhesion, even under high humidity conditions.

To discern the influence of humidity, we conducted experiments at intermediate humidity levels of 40% and 60% while maintaining a constant drying duration of Δt = 24 h and a temperature of T = 35 °C (Fig. 6). As evident from the figure, the detachment force initially declines with rising humidity levels until H = 60%. However, it experiences a substantial increase for a humidity of H = 80%. To better highlight this behaviour, we have included an inset within the figure. This inset portrays the force $F_{d50\%}$, necessary for detaching 50% of the particles and which we derived from the logistic functions. This inset shows $F_{d50\%}$ as a function of the humidity levels. Each data point exhibits the corresponding $F_{d50\%}$ value (in nN). Notably, a marked increase is observed at the highest tested humidity level (80%) at T = 35 °C. This sharp rise may reflect a change in the dominant physical mechanisms such as enhanced capillary condensation that may strengthen the interaction between the particle and the substrate under high humidity conditions.

Finally, to discern the influence of temperature, we conducted experiments at intermediate heat levels of 50 °C, 57.5 °C and 65 °C while maintaining a constant drying duration of Δt = 24 h and humidity of H = 20% (Fig. 7). An increase in temperature leads to an initial rise in F_d, which then appears relatively constant across intermediate temperatures of 50 °C, 57.5 °C, and 65 °C, yet exhibits a notable surge at T = 80 °C. Interestingly, the higher the temperature, the flatter the Gaussian function of the force distribution, suggesting a wide variation of F_d. Again, to better visualize the effect of the temperature, an inset plot of $F_{d50\%}$ is given in the figure.

4 Discussion

To provide a comprehensive summary of the findings on the effect of drying duration presented in Fig. 4 through Fig. 7,
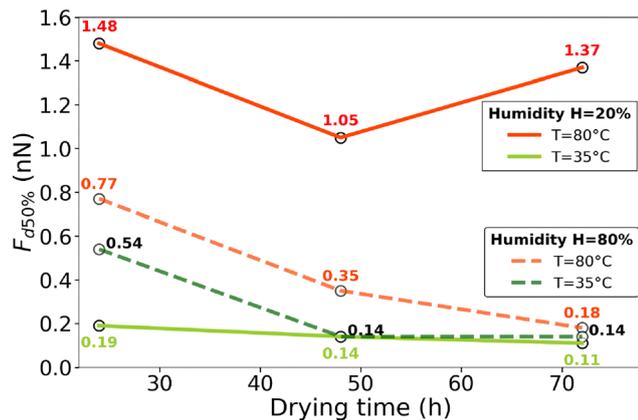
Fig. 8 Effect of drying duration under constant temperature and relative humidity.

Fig. 9 A scanning electron microscope (SEM) image of silver coated silica microspheres (SiO2MS-AG-4.1, Cospheric).

we illustrate in Fig. 8 the detachment force $F_{d50\%}$ required to remove 50% of the microparticles as a function of drying time, Δt. This figure compiles data from the extreme tested drying conditions, specifically at temperatures of 35 °C and 80 °C, and relative humidities of 20% and 80%. As mentioned before, the determination of $F_{d50\%}$ is derived from the logistic function fits, specifically at the point where $P(x) = 50\%$. The insights from Fig. 8 reveal multiple observations based on $F_{d50\%}$ at various durations under constant temperature or relative humidity. Firstly, higher temperatures correspond to increased detachment forces. Secondly, there is a trend of decreased detachment force with rising Δt, although an exception arises at $T = 80$ °C with $H = 20\%$, showcasing an initial decline followed by an increase. Nonetheless, the general trend displays lower $F_{d50\%}$ after 72 h compared to 24 h (third observation). Fourthly, at a relative humidity of $H = 80\%$, the disparity in $F_{d50\%}$ values between experiments conducted at $T = 35$ °C and $T = 80$ °C appears to diminish over time, nearly vanishing at the 72-hour mark. Furthermore, at the longest tested duration of 72 hours, the discrepancy in $F_{d50\%}$ values for experiments at $H = 80\%$, as well as the case of $T = 35$ °C at $H = 20\%$, remains more or less in the same range. This stands in contrast to experiments carried out at $T = 80$ °C at $H = 20\%$. These findings suggest that over time, the impact of drying at various humidity levels becomes less significant compared to the influence of temperature.

The observations above suggest that lower temperatures combined with longer drying durations under high humidity conditions may significantly enhance particle removal and surface cleaning efficiency. The observed variation in detachment force could result from the combined effects of chemical bonding and time-dependent changes in the physical contact between the particle and the substrate. Fig. 9 presents a scanning electron microscope (SEM) image of the particles used in the experiments. It reveals that the silver-coated particles exhibit a rough surface, likely resulting from the coating process during manufacturing. However, this surface roughness is not expected to alter their hydrophilic behavior, and may even help prevent bubble entrapment between the particle
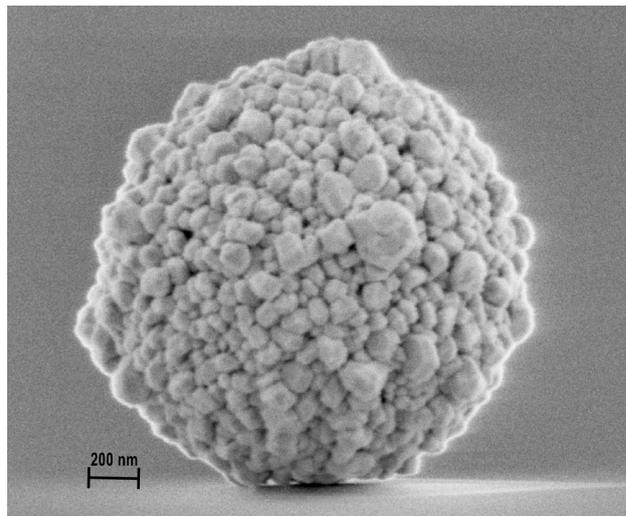
and the hydrophilic substrate upon immersion.[23] To explore how the contact area between the particle and substrate evolves with drying time, we analyzed two conditions: $T = 80$ °C at $H = 20\%$ and $T = 35$ °C at $H = 80\%$.

The results are presented in Fig. 10, which shows the measured contact length obtained from SEM imaging. Due to the irregular and rough morphology of the particles, the contact zone cannot be approximated as a perfect circular disk. Consequently, we characterize the contact by a representative contact length. Although each measurement captures only a two-dimensional cross-section, the full dataset for each condition effectively samples the 360° contact perimeter. For each drying condition, all individual data points are shown in a neutral color, while the mean and median values are highlighted with colored square and star markers, respectively, to emphasize the overall trend. Additionally, colored lines are used to indicate the mean trend for each condition. Notably, under the drying condition of $T = 80$ °C and $H = 20\%$, the average contact length initially decreases and then increases over time. This evolution mirrors the trend observed in the detachment force $F_{d50\%}$ under the same conditions. Such a correlation suggests that variations in the contact area may influence the detachment force. However, this trend is not observed under the condition of $T = 35$ °C and $H = 80\%$. Although the contact length decreases between $\Delta t = 24$ h and $\Delta t = 48$ h and remains smaller than that measured at $T = 80$ °C, $H = 20\%$ for the same time points—consistent with the lower corresponding detachment force (cf. Fig. 8)—it then increases and reaches a magnitude comparable to that of the higher temperature condition.

To validate the hypothesis linking drying conditions to changes in both the contact area and chemical bonding, which may in turn affect the detachment force, a more in-depth investigation of the particle's mechanical properties and potential chemical interactions would be required. These aspects lie beyond the scope of the present study and will be
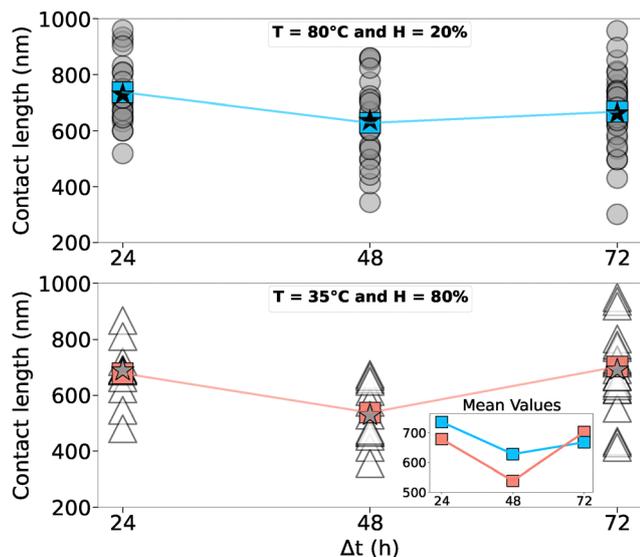
Fig. 10 Contact size at the base of the particle for experiments conducted at $T = 80\ °C$, $H = 20\%$ (top) and $T = 35\ °C$, $H = 80\%$ (bottom). Each data series, comprising between 11 and up to 32 points, is displayed with individual data points in neutral colors, and mean/median values highlighted by colored square and star markers, respectively. The inset compares the mean trends from the two main panels.
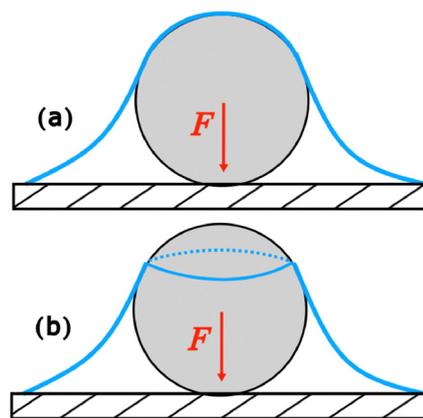

Fig. 11 Schematic representation of forces acting on a microparticle during drying. (a) When the particle is fully immersed, only the Laplace pressure acts uniformly around it. (b) As drying progresses and a capillary bridge forms, both the Laplace pressure and capillary forces contribute to pressing the particle against the substrate.

the focus of future work. Nonetheless, the comparison of detachment forces $F_{d50\%}$ under "fast drying" conditions (i.e., $T = 80\ °C$, $H = 20\%$) and 'slow drying' conditions (i.e., $T = 35\ °C$, $H = 80\%$) at drying durations of $\Delta t = 24$ h and 48 h offers strong indications of particle deformation occurring during drying. In addition, contact length measurements across different drying durations (Δt) reveal variations that reflect evolving particle–substrate interactions. In parallel, Fig. 8 shows a consistent decrease in $F_{d50\%}$ values between 24 h and 48 h across nearly all conditions, with nearly identical rates of decrease, except for the case of $H = 20\%$ and $T = 35\ °C$. This trend suggests that the particles may experience a relaxation phase following compression that would have occurred earlier during drying. Such compression could result from capillary bridges that form between the particle and the substrate, pulling the particle toward the surface and increasing the contact area. Interestingly, this effect appears to depend strongly on the environmental conditions: at high temperature and low humidity, the detachment force is notably higher, indicating stronger capillary forces during drying. Conversely, at high temperature and high humidity, the detachment force is significantly lower, suggesting that large capillary forces may not sufficiently develop in these conditions, possibly due to slower evaporation or altered bridge formation dynamics.

This capillary-induced "compression" mechanism appears reminiscent of the phenomenon described by Ipatova et al.,[23] where a trapped bubble beneath an immersed microparticle exerts forces that either retain the particle against the substrate or contribute to its removal. In our case, the evolution of the detachment force, together with the measured variations in contact area, supports a scenario in which particles experience

an initial compression during drying, followed by partial relaxation within the first 48 hours. The schematic in Fig. 11 depicts the compression experienced by a particle throughout the drying process. When the particle is fully wetted, the compressive force arises solely from the Laplace pressure (Fig. 11(a)). As drying proceeds and a capillary bridge forms, an additional capillary force develops, that may further pressing the particle against the substrate (Fig. 11(b)).

Additional evidence of this compression comes from the Gaussian distributions of detachment force data, which are notably narrower at lower drying temperatures (Fig. 5(a)). This suggests reduced variability and more uniform contact behavior under milder drying conditions. In contrast, higher temperatures—especially under low humidity—appear to promote stronger particle deformation during drying, potentially due to more pronounced capillary effects. This may result in increased contact areas, enhanced spreading, and ultimately, higher adhesion forces.

5 Conclusion

In this study, we investigated the detachment force required to remove a hydrophilic microparticle from a hydrophilic substrate after a controlled drying step. This specific surface combination was deliberately chosen to avoid bubble entrapment, a phenomenon previously shown to strongly affect detachment forces when either surface is hydrophobic.[23] The drying step was conducted under various environmental conditions, including changes in air temperature, relative humidity, and drying duration.

Our findings reveal that while decreasing humidity tends to increase the detachment force, the effect of temperature is considerably more pronounced. Furthermore, increasing the drying duration generally leads to a reduction in detachment force, except under the condition of low humidity combined with high temperature, where stronger adhesion is observed. A

key result of this work is the identification of a link between drying conditions and the evolution of the contact area between the particle and the substrate, as measured by SEM imaging. The contact length was found to vary over time, suggesting that drying may induce capillary-driven compression of the particle, followed by a relaxation phase. This trend was consistently observed across most of the tested conditions during the first 48 hours of drying and is further supported by the narrowing of Gaussian distributions of detachment force at lower temperatures, indicative of more uniform contact behavior.

Where earlier studies focused on the effects of individual parameters such as temperature or humidity on adhesion,[19–22] our results reveal a more integrated picture. The interplay between temperature, humidity, and drying duration shows that adhesion cannot be explained by a single factor alone. Instead, it arises from the coupled influence of evaporation dynamics, capillary stress buildup, and interfacial deformation. This study thus extends previous work by showing how drying history shapes the mechanical state of the particle–substrate contact, providing a unified framework for understanding drying-induced adhesion.

Beyond its experimental insights, this work also highlights the need to incorporate history-dependent effects into theoretical models of adhesive contact. Classical approaches such as JKR,[14] DMT,[15] and their later extensions[16–18] successfully describe static elastic interactions but do not yet account for the evolving contact geometry and stress redistribution induced by drying. The present findings therefore lay the groundwork for developing next-generation adhesion models that bridge static contact mechanics with time-dependent, capillarity-driven processes.

Finally, regarding potential applications, our results suggest that cleaning processes involving hydrophilic particles on hydrophilic surfaces may benefit from operating at lower temperatures—regardless of humidity level—as this facilitates particle removal while reducing energy input. When humidity is limited, extending the drying duration may further enhance cleaning efficiency by promoting particle relaxation and decreasing adhesion strength. This finding contrasts with conventional industrial practices that rely on elevated temperatures for cleaning and opens promising avenues for energy-efficient surface hygiene strategies. It should be emphasized, however, that these conclusions apply specifically to systems where both the particle and the substrate are hydrophilic. As shown previously,[23] mixed wettability can lead to bubble entrapment and drastically alter adhesion. Future work will address such scenarios and further probe capillary-induced contact deformation, encompassing both mechanical compression and chemical bonding, as central determinants of detachment behavior.

Author contributions

FZ: conceptualization, funding acquisition, project administration, supervision, formal analysis, investigation, methodology,

validation, visualization, writing – original draft, writing – review & editing. JS: investigation, data curation, and writing – review & editing. AI: data curation. AD: conceptualization, investigation, and writing – review & editing. HNY, IU, GD: conceptualization & funding acquisition. CF: conceptualization, funding acquisition & methodology. PM: conceptualization, funding acquisition, methodology & supervision.

Conflicts of interest

There are no conflicts to declare.

Data availability

Supplementary information includes details of the calibration of the micropipette tip area from electrical resistance measurements, the method used to calculate the detachment force from the applied pressure, a description of the supplementary video illustrating a microparticle detachment experiment, and all fitted parameters of the logistic regressions corresponding to the figures in the main text. See DOI: https://doi.org/10.1039/d5sm01109d.

Data for this article are available at Zenodo at https://doi.org/10.5281/zenodo.17021568.

Acknowledgements

Notes and references

1 H. F. Okorn-Schmidt, F. Holsteyns, A. Lippert, D. Mui, M. Kawaguchi, C. Lechner, P. E. Frommhold, T. Nowak, F. Reuter, M. B. Piqué, C. Cairos and R. Mettin, *ECS J. Solid State Sci. Technol.*, 2014, **3**, N3069–N3080.

2 D. W. Cooper, *Aerosol Sci. Technol.*, 1986, **5**, 287–299.

3 F. Tardif, A. Danel and O. Raccurt, *J. Telecommun. Inf. Technol.*, 2005, **nr 1**, 11–19.

4 R. A. Bowling, *J. Electrochem. Soc.*, 1985, **132**, 2208.

5 Y. Taga, *CIRP Ann. Manuf. Technol.*, 1997, **218**, 335–341.

6 K. Bewilogua, G. Bräuer, A. Dietz, J. Gäbler, G. Goch, B. Karpuschewski and B. Szyszka, *CIRP Ann. Manuf. Technol.*, 2009, **58**, 608–627.

7 M. Mauermann, U. Eschenhagen, T. Bley and J. P. Majschak, *Trends Food Sci. Technol.*, 2009, **20**, S9–S15.

8 M. Basso, M. Simonato, R. Furlanetto and L. De Nardo, *J. Ind. Eng. Chem.*, 2017, **53**, 23–36.

9 J. M. Vicaria, E. Jurado-Alameda, O. Herrera-Márquez, V. Olivares-Arias and A. Ávila-Sierra, *J. Cleaner Prod.*, 2017, **168**, 87–96.

10 M. W. L. Chee, T. V. Ahuja, R. K. Bhagat, N. Taesopapong, S. A. Wan, R. L. Wigmore and D. I. Wilson, *Food Bioprod. Process.*, 2019, **113**, 142–153.

11 A. Ipatova, PhD thesis, Université de Lille, IEMN, 2023.

12 F. Giorgiutti-Dauphiné and L. Pauchard, *Eur. Phys. J. E:Soft Matter Biol. Phys.*, 2018, **41**, 32.

13 L. Pauchard, *Europhys. Lett.*, 2006, **74**, 188.

14 K. L. Johnson, K. Kendall and A. D. Roberts, *Proc. R. Soc. London, Ser. A*, 1971, **324**, 301–313.

15 B. Derjaguin, V. Muller and Y. Toporov, *J. Colloid Interface Sci.*, 1975, **53**, 314–326.

16 D. Maugis, *J. Colloid Interface Sci.*, 1992, **150**, 243–269.

17 J. A. Greenwood, *Proc. R. Soc. A*, 1997, **453**, 1277–1297.

18 R. W. Carpick, D. Ogletree and M. Salmeron, *J. Colloid Interface Sci.*, 1999, **211**, 395–400.

19 C. Faille, I. Bihi, A. Ronse, G. Ronse, M. Baudoin and F. Zoueshtiagh, *Colloids Surf., B*, 2016, **143**, 293–300.

20 R. Shiri, A. Ahmadi-Dehnoei and S. Ghasemirad, *J. Adhes.*, 2024, **100**, 34–62.

21 A. Thill and O. Spalla, *Langmuir*, 2002, **18**, 4783–4789.

22 Y. Endo, Y. Kousaka and H. Onitsuka, *KONA Powder Part. J.*, 1995, **13**, 215–222.

23 A. Ipatova, A. Duchesne, H. N. Yoshikawa, P. Mariot, C. Leroy, C. Faille, I. Ueno, G. F. Dietze and F. Zoueshtiagh, *Phys. Rev. Fluids*, 2024, **9**, 084301.

24 C. Faille, C. Lemy, A. Allion-Maurer and F. Zoueshtiagh, *Colloids Surf., B*, 2019, **182**, 110398.

25 S. Derouiche, P. Mariot, M. Warnier, E. Vancauwenberghe, G. Bidaux, P. Gosset, B. Mauroy, J.-L. Bonnal, C. Slomianny, P. Delcourt, E. Dewailly, N. Prevarskaya and M. Roudbaraki, *Cancer Prev. Res.*, 2017, **10**, 177–187.

26 O. P. Hamill, A. Marty, E. Neher, B. Sakmann and F. J. Sigworth, *Pfluegers Arch.*, 1981, **391**, 85–100.

27 R. D. Deegan, *Phys. Rev. E*, 2000, **61**, 475–485.